Simulation and Measurement of the Magnetic Field Coupling From a Proximity Detection System to Trailing Cables

Chenming Zhou, Bruce Whisner, and Jacob Carr

***Abstract*—Some of the common and serious hazards in underground mines are the dangers of being pinned, crushed, or struck by a large mining machine such as a scoop or a continuous mining machine (CMM). Proximity detection systems (PDSs) have been applied to protect miners from these hazards. The primary components of PDSs that are currently approved by the Mine Safety and Health Administration (MSHA) for use in underground coal mines are machine-mounted magnetic field generators and a miner-worn component (MWC), which measures the strength of the magnetic fields produced by the generators. Since these systems are magnetic field based, they can be adversely impacted by nearby cables due to parasitic coupling. Some mobile equipment in underground mines is electrically powered by long trailing cables that are pulled through the mine behind the equipment. Because the components of the PDS (generators and MWC) are frequently in close proximity to these cables, parasitic coupling can occur. Researchers from the National Institute for Occupational Safety and Health investigated the influence of trailing cables on the performance of PDSs. In particular, a three-phase model was proposed to describe the coupling process. The factors for controlling the magnetic field coupled from a field generator to a trailing cable were experimentally studied. The results show that the coupling is primarily controlled by two factors: the distance between the PDS components and the cable and the impedance between the cable and the ground. The coupling can be mitigated by either maintaining some minimum separation distance between the PDS components and the cable or increasing the impedance between the cable and the ground. The results presented in this article can help PDS manufacturers to design systems that are more immune to these effects.**

***Index Terms*—Magnetic field tracking, parasitic coupling, proximity detection.**

I. Introduction

DUE to the limited space and visibility in underground coal mines, operation of continuous mining machines (CMMs) has historically been a hazardous job. From 1984 to 2015, an average of 250 injuries occurred every year in the United States during operation of CMMs, and 43 miners have been killed by striking or pinning accidents involving CMMs [2]. Additionally, there have been ten fatal accidents involving mobile haulage equipped with trailing cables from 2000 to 2015 [3]. In response to these fatalities and injuries, the Mine Safety and Health Administration (MSHA) promulgated a regulation in 2015 requiring the use of a proximity detection system (PDS) on all CMMs except on full-face machines.

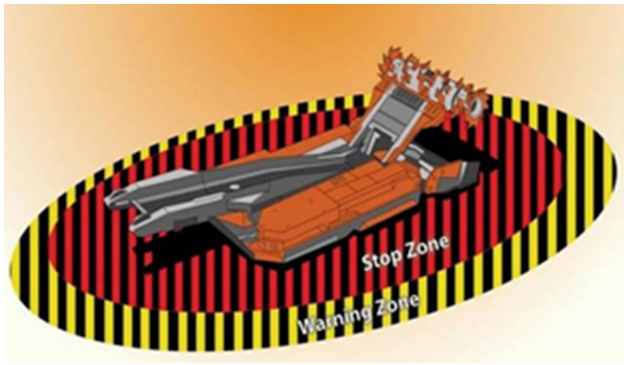

Fig. 1. PDS installed on a CMM establishes a stop and warning zone around a CMM to protect miners from the pinning and striking hazards [1].

To meet MSHA's requirement, a PDS must cause a machine to stop before contacting a miner and provide an audible and visual warning signal that alerts miners before the system causes a machine to stop. Fig. 1 shows an example of a PDS installed on a CMM. The PDS establishes a stop and warning zone around the CMM to protect miners from the pinning and striking hazards.

In the regulation, MSHA did not specify the technology that should be used for proximity detection. However, currently all PDSs approved for underground coal mines are magnetic field based. A magnetic-field-based PDS contains two major components: the machine-mounted magnetic field generator that creates fields around the machine and the miner-wearable component (MWC) that reads the flux density of a generator. These PDSs use the magnetic field readings from the MWC to determine whether a miner is at a safe distance from the machine. A stable magnetic field distribution is essential for the accuracy and reliability of a PDS.

Ideally, the magnetic field radiated from a field generator should only depend on the distance between the generator and

Manuscript received July 9, 2019; revised February 28, 2020; accepted March 20, 2020. Date of publication April 13, 2020; date of current version July 1, 2020. Paper no. 2019-MIC-0826.R1, presented at the 2019 IEEE Industry Applications Society Annual Meeting, Baltimore, MD, USA, Sep. 29–Oct. 3, and approved for publication in the IEEE TRANSACTIONS ON INDUSTRY APPLICATIONS by the Mining Industry Committee of the IEEE Industry Applications Society. *(Corresponding author: Chenming Zhou.)*

The authors are with the Centers for Disease Control and Prevention, National Institute for Occupational Safety and Health, Pittsburgh, PA 15236 USA (e-mail: czhou@cdc.gov; uwo3@cdc.gov; hwh1@cdc.gov).

Color versions of one or more of the figures in this article are available online at https://ieeexplore.ieee.org.

Digital Object Identifier 10.1109/TIA.2020.2987541

the MWC. This is, however, not always the case when a PDS operates in complex mining environments. Particularly, MSHA, PDS manufacturers, and mine operators have noticed that a PDS can produce false alarms when operating in close proximity to trailing cables. Such false alarms may compromise the confidence of miners using the system**.** In addition, a high number of false alarms will lead to miner alarm fatigue, which can result in desensitization to alarms and missed alarms, which eventually lead to serious safety concerns [4]. As a result, the influence of trailing cables should be mitigated when possible.

II. Related Work

The influence of trailing cables on the performance of a magnetic PDS is mainly caused by the parasitic (inductive) coupling between the PDS and the cables [5], [6]. The problem of field coupling from a PDS to a trailing cable shares great similarities with the field-to-transmission line coupling problem that has been extensively investigated in the past decades, primarily from the theoretical modeling perspective [7]–[13]. The field-to-transmission line research was mainly driven by the electromagnetic compatibility (EMC) applications where lightning-induced voltages on overhead power or telecommunication lines [11] and electromagnetic interference coupling between power cables and sensitive circuits are of concern [7]. A variety of models, such as the transmission line approach and antenna model [9], [10], have been developed to calculate the field-to-transmission line coupling. While most of the developed models assume a uniform excitation electromagnetic field arriving from a distant source (e.g., lightning), the research presented in [13] and [14] is based on a nonuniform magnetic field source excited by a loop antenna, which is more related to the problem of trailing cable coupling that is studied in this article.

Another group of published works that is related to trailing cable coupling is medium frequency (MF) communications. Instead of mitigating trailing cable coupling, an MF communication system takes advantage of the parasitic coupling by using existing conductors, such as rail tracks, power cables, and water pipes in mines, as the communication medium for voice and data communications [15]. As a result, for MF communication applications, the goal is to create a favorable condition for parasitic coupling so that the coupled signal can be maximized rather than being minimized. Research has been conducted to investigate magnetic fields coupled from a transmission line to a loop antenna [16], and methods were developed to characterize the coupling from a ferrite-cored rod antenna to a conductor [17].

In addition to trailing cables, magnetic fields from a PDS can be coupled to other existing conductive structures in the underground. For example, it is shown in [18] that steel mesh used for roof support can significantly enhance the magnetic fields from a PDS and cause the corresponding detection zone size to be increased. Some FEKO-based simulation results pertaining to the influence of steel mesh on the performance of PDSs are presented in [19]. The influence of *in situ* coal (which might be conductive) has been investigated in [20] and the result shows that the situ coal has no significant impact on the magnetic field distribution.

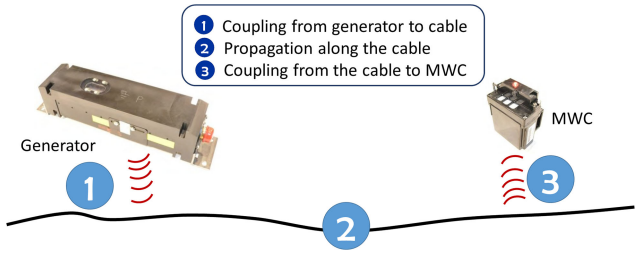

Fig. 2. Parasitic coupling between a PDS and a trailing cable can be virtually decomposed into three phases.

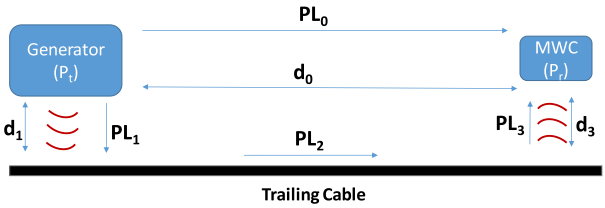

Fig. 3. Link budget for a magnetic proximity system with the presence of a trailing cable.

This article mainly presents a set of laboratory experiments designed by National Institute for Occupational Safety and Health (NIOSH) researchers, in which a commercial PDS is used to investigate, quantify, and develop mitigation strategies for PDS performance inconsistencies caused by parasitic coupling associated with trailing cables. In addition, some FEKO-based simulation results are presented to show the influence of frequency on the parasitic coupling.

III. Coupling Between a PDS and a Trailing Cable: Link Budget Analysis

As shown in Fig. 2, the parasitic coupling between a PDS and a trailing cable can be decomposed into the following three phases:

1) magnetic field couples from a field generator to a nearby cable;
2) the coupled magnetic field propagates along the cable;
3) magnetic field couples from the cable to a nearby MWC.

There are energy losses involved in each of the three phases shown in Fig. 2. The energy loss for each of the phases is then represented by PL_i where "i" is the index of the phase. As shown in Fig. 3, for a PDS operating in close proximity to a trailing cable, the signal $r(t)$ received by an MWC consists of two components and can be expressed as

$$r\,(t)\ = r_{\mathrm{dr}}\ (t) + r_{\mathrm{cp}}\,(t) \tag{1}$$

where $r_{\mathrm{dr}}(t)$ is the desired target signal, which is radiated directly from the corresponding proximity generator, and $r_{\mathrm{cp}}(t)$ denotes the signal received from the trailing cable due to the parasitic coupling.

For proximity detection applications, $r_{\mathrm{cp}}(t)$ is undesired and should be minimized. In reality, however, the two signals are always mixed with each other and cannot be easily separated. The

two received signals $r_{\rm dr}(t)$ and $r_{\rm cp}(t)$ are combined coherently at the receiver as they are from the same signal source, similar to the fact that multipath components in a UHF radio channel are summed based on their voltages, not power [21].

Although practically $r_{\rm dr}(t)$ and $r_{\rm cp}(t)$ are always mixed, theoretically, they can be treated as two separated signals/links and can be analyzed independently. To be consistent with conventional link budget analysis, we will investigate the received power rather than the magnetic field (induced voltage) for each link. The received power (in a logarithmic scale) for the direct link $P_{\rm dr}$ (associated with signal $r_{\rm dr}(t)$ can be obtained by

$$P_{\rm dr} = P_t \ - PL_0\left(d_0\right) \tag{2}$$

where P_t is the transmitted power determined by a variety of parameters, such as the electric current fed to the transmitter antenna, as well as the transmitter antenna properties (i.e., coil radius and number of turns) [22]. For a given frequency, the path loss $\rm PL_0$ is mainly determined by the distance between the generator and the MWC d_0. Assuming a constant P_t and with the absence of trailing cables, a PDS uses $P_{\rm dr}$ for determining the location (or zone) of an MWC.

As illustrated in Fig. 3, the received power for the second link (the trailing cable coupling link) can be expressed as

$$P_{\rm cp} = P_t \ - {\rm PL}_1\left(d_1\right) - {\rm PL}_2\left(d_2\right) - {\rm PL}_3\left(d_3\right) \tag{3}$$

where $\rm PL_1$, $\rm PL_2$, and $\rm PL_3$ represent the energy loss associated with the coupling from the generator to the trailing cable, propagation along the trailing cable, and the coupling from the trailing cable to the MWC, respectively. The path loss for each stage $\rm PL_i$ is determined by the corresponding distance d_i—the greater the distance, the larger the path loss. One of the focuses of this article is to investigate how $\rm PL_i$ varies with the distance d_i at each stage.

When the undesired signal $P_{\rm cp}$ is comparable to the target signal $P_{\rm dr}$, the position/zone estimation provided by the PDS will be incorrect. The worst scenario occurs when $P_{\rm cp}$ is significantly greater than $P_{\rm dr}$, in which case nuisance alarms may be triggered. This is the case when the MWC is physically located far from the generators (i.e., when d_0 is large) but close to a trailing cable (i.e., when d_3 is small).

In addition to the distance factor in each phase, there is another important factor that can influence the PDS and trailing cable coupling: the impedance of the loop (network) formed by the cable. It is known that the magnetic field detected by an MWC close to a trailing cable is due to the induced current in the cable, which is produced by the electromotive force (EMF) caused by a changing magnetic field from a PDS generator. Fig. 4 shows a simplified model for calculating the induced current in the cable for a given EMF ε. Trailing cables are typically used to power heavy-load mining equipment. As a result, one end of the trailing cable is connected to a power center, and the other end is connected to mining equipment such as a CMM. As shown in Fig. 4, at the power center end, the cable is directly connected to the earth ground, while at the CMM end, the cable is connected to the earth ground through a complex impedance *X*, primarily due to the capacitance between the large metallic machine frame and the earth. In the network there might be some other impedances

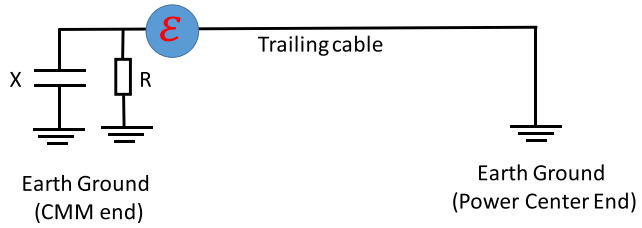

Fig. 4. Simplified model for calculating the induced current on a trailing cable due to the parasitic inductive coupling from a PDS generator to a trailing cable.

due to the existing inductance and resistance. Those impedances, however, have been ignored in this simplified model.

In order to investigate how the coupled magnetic field varies with the impedance between the CMM and the earth, a potentiometer has been introduced to the system so that the impedance between the CMM and the earth can be varied by adjusting the resistance of the potentiometer with a controlled accuracy. With the manually introduced potentiometer, which is shown in Fig. 4 as "*R*," the induced current in the trailing cable can be computed as

$$I_c = \ \varepsilon\left(\frac{1}{R} + \frac{1}{jX}\right) \tag{4}$$

where *R* is the resistance of the potentiometer. The EMF ε can be expressed as

$$\varepsilon \ = -M_{\rm sc}\ \frac{dI_s}{dt} = 2\pi f M_{sc}\, I_s \tag{5}$$

where f is the frequency, I_s is the source current carried by the PDS generator antenna, and M_{sc} is the mutual inductance between the PDS generator antenna and the coupling circuits, which usually cannot be expressed in an analytical formula. In this case, M_{sc} is determined by geometrical factors such as the distance between the generator and the cable, the orientation of the cable relative to the generator antenna.

The magnitude of the induced current can be expressed as

$$|I_c| = \frac{\varepsilon\sqrt{R^2 + X^2}}{RX}. \tag{6}$$

It is known that the magnetic field radiated from the cable is proportional to the current in the cable. As a result, the magnetic field received by an MWC can be calculated as

$$|B| = K_0\ \frac{\sqrt{R^2 + X^2}}{RX} \tag{7}$$

where K_0 is a constant determined by different factors such as the source current, frequency, the distance between the generator and the cable, and the distance between the cable and the MWC. In reality, both K_0 and *X* are most likely unknown and cannot be easily measured. To validate this model, a series of measurements can be made by changing the resistance *R* and monitoring the change of the magnetic field *B*, while keeping the value of K_0 and *X* the same. K_0 and *X* then will be used as two fitting parameters to best fit the modeling result to the measured result.

In summary, the major controlling factors of the coupled magnetic field *B* given in (7) are as follows:

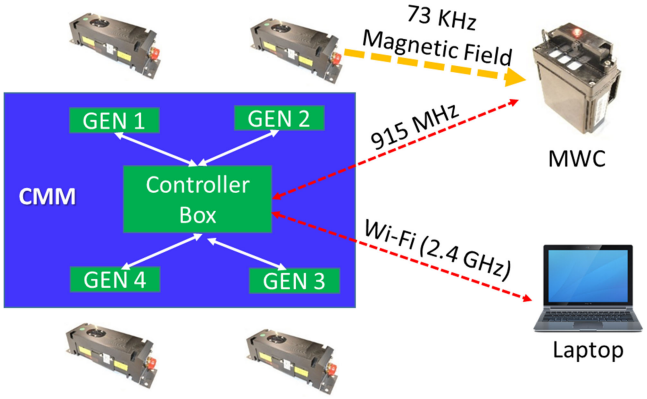

Fig. 5. Experimental setup for measuring coupled magnetic fields.

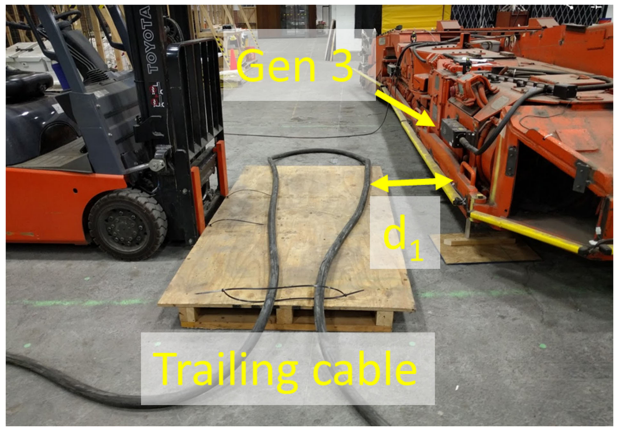

Fig. 6. Experimental setup for measuring how the coupled field varies with the distance between the cable and the generator.

1) source current I_s;
2) orientation of the cable relative to the generator antenna;
3) distance between the generator and the cable (d_1);
4) frequency (f);
5) distance between the cable and the MWC (d_3);
6) impedance of the coupling network (*R, X*).

It is known that the influence of the first controlling factor is straightforward as the coupled magnetic field linearly increases with the source current I_s. The second and the third factors are closely related to each other so we will only focus on one of them. As a result, in the rest of the article, we will mainly study the controlling factors of d_1, f, d_3, *R*, and *X*.

IV. Measuring the Parasitic Coupling Between a PDS and a Trailing Cable

A. Experimental Setup

Fig. 5 illustrates the general experimental setup for measuring the coupled magnetic fields, based on a commercial PDS used in underground coal mines. The PDS has four generators (labeled from Gen 1 to Gen 4) installed on the two sides of the CMM. Each generator transmits a short duration of magnetic field signal at a frequency of 73 KHz in a known sequential order. An MWC is used to measure the three axes (i.e., *X*, *Y*, and *Z*) of the magnetic field. The magnetic fields measured by the MWC are wirelessly (915 MHz) transmitted back to a controller box installed on the CMM in real time. A laptop is then used to wirelessly (2.4 GHz) read the measured magnetic fields from the controller box through a LabVIEW program. The trailing cable is a standard shielded, heavy-duty cable that consists of five conductors.

It should be noted that the measured magnetic field in this article is shown as a digital number from an analog-to-digital converter without a specific unit. These digital numbers, however, can be converted to true magnetic field values with either a unit of Tesla or Gauss by multiplying a constant, which can be obtained through appropriate calibrations.

The magnetic field readings (i.e., digital numbers without a unit) provided by the MWCs are generally not accessible by their users for a PDS used in coal mines. For the purpose of research, however, we have utilized a modified PDS by adding an interface through which the magnetic field information can be accessed by a computer. More details about these modifications to a PDS designed at NIOSH can be found in [23]–[25].

One of the challenges for measuring the coupled field is to separate the coupled field $r_{\mathrm{cp}}(t)$ from the direct transmitted field $r_{\mathrm{dr}}(t)$. In our measurements, this is achieved by purposely placing the MWC close to the trailing cable but far away from all four generators. Under such a configuration, $r_{\mathrm{dr}}(t)$ is negligible compared to $r_{\mathrm{cp}}(t)$ so that the measured magnetic field is mainly the coupled field. This assumption can be quickly verified in the field by slightly moving the MWC away from the cable and monitoring the change on the measured magnetic field. If the field quickly decays as the MWC moves away from the cable, it can be determined that the source of the field is the cable, not a field generator.

It should be noted that during the measurements the orientation of the MWC is generally not a concern as the measured three-axis magnetic fields were combined and the vector sum value was used to represent the magnetic field value at that specific location.

B. Measuring the Magnetic Field Variation With the Distance Between the Field Generator and the Trailing Cable

Fig. 6 shows the experimental setup for measuring how the coupling loss PL_1 varies with d_1, which is the distance between the field generator and the cable. One section of the trailing cable was purposely placed close to one of the four generators (Gen 3) to facilitate the coupling from the generator to the cable. A forklift was used to move the cable so that the distance between the cable and the generator can be varied. The coupled magnetic fields for different distances were recorded by an MWC located far away from the Gen 3 but directly against the cable (i.e., $d_3 \approx 0$).

C. Measuring the Magnetic Field Variation Along the Trailing Cable

Fig. 7 shows the experimental setup for measuring how PL_2 varies with the distance d_2. For every two meters, a marker was made along the cable using a white chalk. The MWC was placed

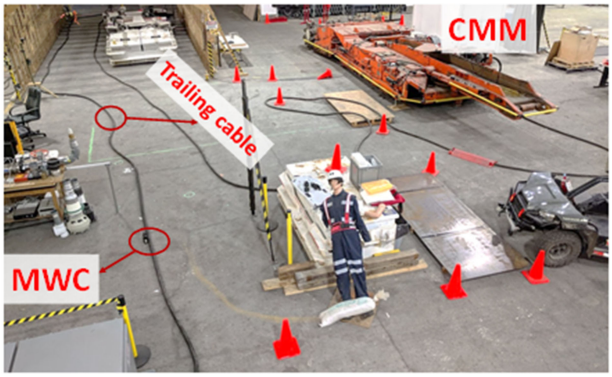

Fig. 7. Experimental setup for measuring how the coupled field attenuates along the cable.

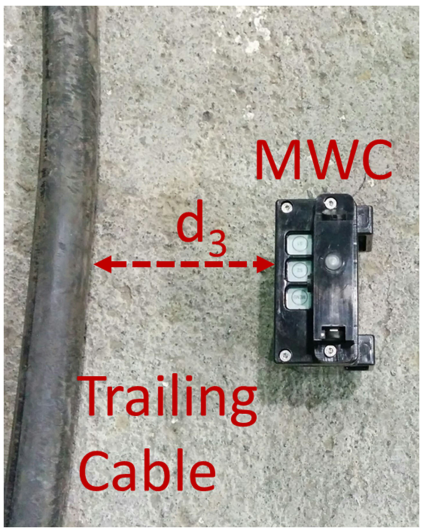

Fig. 8. Experimental setup for measuring how the coupled field varies with the distance between the cable and the MWC.

directly against the cable ($d_3 = 0$) at those marked locations to measure the coupled magnetic field along the trailing cable.

D. Measuring the Magnetic Field Variation With the Distance Between the Cable and the MWC

Fig. 8 shows the experimental setup for measuring how PL_3 varies with the distance d_3. The MWC was moved away from the cable with a step size of 2 cm, and the coupled field was recorded at every stop. During this measurement, all other parameters (except the distance d_3) that can possibly affect the coupled field remained the same.

E. Measuring the Magnetic Field Variation With the Impedance Between the CMM and the Ground

CMMs typically have a large metallic pan (see Fig. 9) that is designed to hold the coal cut from the cutting drum. The impedance (particularly, the capacitance) between the CMM and the ground is affected by the height of the PAN from the floor. Fig. 9 shows two different configurations where the PAN was raised to different levels to alter the impedance between the CMM and the ground. In the "PAN UP" configuration, the pan and the drum were raised up from the ground so the impedance X (as shown in Fig. 4) was increased. In the "PAN DOWN" configuration, the pan and the drum were dropped to the floor so that the impedance X was decreased. In each configuration, the metallic frame of the CMM was connected to the earth ground with a wire, and a potentiometer was added to vary the resistance between the CMM metallic frame and the earth ground.

Fig. 9. Varying the impedance between the CMM and the ground by raising ("PAN UP") and dropping ("PAN DOWN") the metallic pan of the machine.

V. Simulating the Parasitic Coupling Based on FEKO

The PDS used in the measurements reported in this article is a commercial PDS that does not support adjustable frequencies. As a result, some simulation studies were conducted to investigate how frequency affects the parasitic coupling. The simulations were based on FEKO, an EM software that has been used to investigate the magnetic field coupling of MF communications [16] and recently in magnetic PDSs [22].

A picture of the simulated ferrite-rod antenna along with an actual antenna used in a PDS generator is shown in Fig. 17. The simulated antenna was constructed based on the exact parameters of the actual antenna. The geometric parameters of the simulated antenna are listed in Table I. It should be noted that this FEKO-based antenna model has been validated by extensive measurement results in [22]. The antenna was driven by a voltage source.

To simplify the problem, a large rectangular wire loop (50 m $\times$ 5 m) was used to approximate the coupling loop formed by the trailing cable and the power system (as the simplified model shown in Fig. 4). The resistance and the capacitance in Fig. 4 were implemented in FEKO with a complex impedance load. The ferrite-rod antenna was placed 0.1 m from one side of the loop. Fig. 10 shows the simulation setup for investigating how the system frequency affects the parasitic coupling. The receiver is located at (–18.75 m, 5.115 m) with the origin of the coordinate defined in the center of the antenna.

VI. Results and Discussion

A. Measurement Results

Based on experimental setups given in Section IV-A, the three-axis components (i.e., B_x, B_y, and B_z) of the coupled magnetic fields were measured under different configurations designed to study the influence of different parameters. The measured three-axis components were then combined and, unless stated

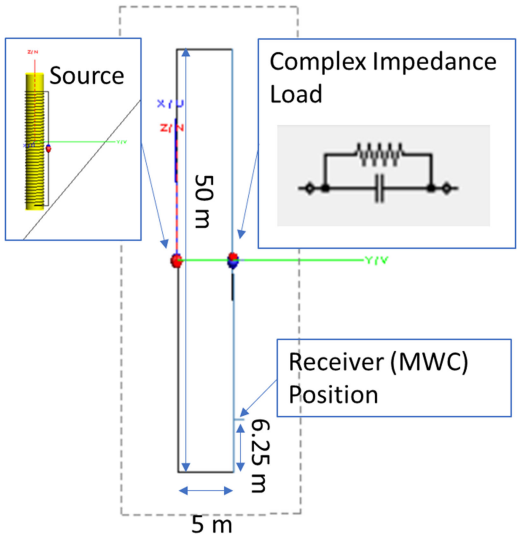

Fig. 10. Simulation setup for investigating how frequency affects the coupled field received by an MWC.

TABLE I
ANTENNA PARAMETERS

Parameter	Value
Radius (a)	12.7 mm
Number of turns (N)	37
Length (L_c)	0.16 m
Ferrite length (L_f)	0.1905 m
Permeability (μ_r)	2500
Wire radius	0.685 mm
Frequency (f)	73.6 kHz

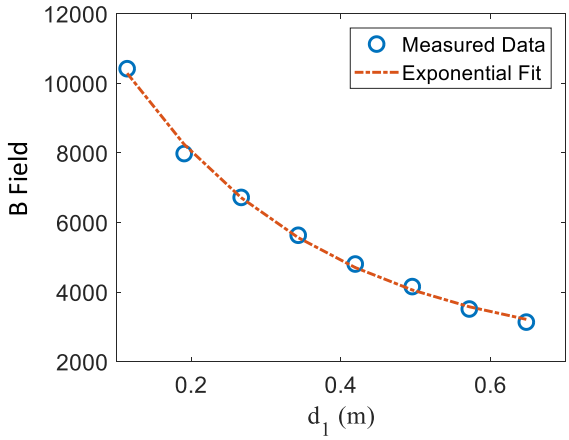

Fig. 11. Coupled magnetic field attenuates with the distance between the cable and Gen 3.

otherwise, only the vector sum of the measured fields were analyzed and are presented in this section.

Fig. 11 shows how the coupled magnetic field variates with the distance between the cable and Gen 3, based on the experimental setup illustrated in Fig. 6. It is shown that the coupled field decreases rapidly with the distance, particularly when the cable is relatively close to the generator (e.g., for $d_1 < 0.2$ m). This

Fig. 12. Picture showing a PDS generator installed too close to the CMM end of the trailing cable which causes strong magnetic field coupling even though the rest of the cable is far from the generator.

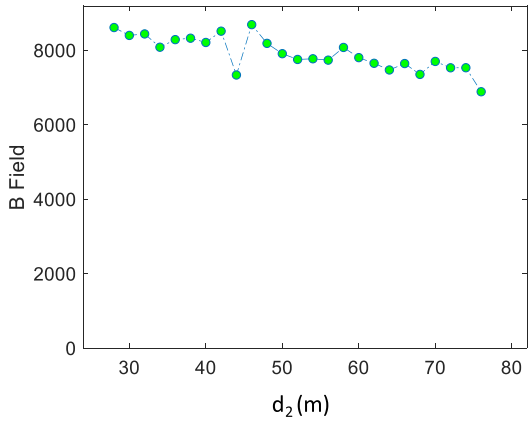

Fig. 13. Coupled magnetic field varies with the distance along the trailing cable.

observation suggests that trailing cables should be kept away from PDS generators in order to mitigate the coupling from the generator to the cable. It is also shown in Fig. 11 that the field approximately attenuated exponentially with the distance.

While under most circumstances, magnetic field coupling can be mitigated by moving around the trailing cable to increase the distance between the cable and the generator, there is one circumstance where the distance between the cable and the generator is primarily determined by the location where the generator is installed and, thus, cannot be easily adjusted. This is the case when a generator is installed close to the end of the trailing cable where the cable connects to the CMM, as shown in Fig. 12. As a result, special care must be taken when one installs PDS generators. If a generator is installed too close to the trailing cable, strong coupling could occur despite that the rest of the cable stays far from the generator.

Fig. 13 shows how the coupled magnetic field varies with the distance along the trailing cable, based on the experimental setup shown in Fig. 7. In contrast to the rapid attenuation observed in Fig. 11, the coupled magnetic field in Fig. 7 does not show significant attenuation with the distance along the cable. This finding is consistent with the conclusion reported in [16] and [26], which concludes that MF signals, after being coupled to a transmission line, show a very small transmission loss along the cable.

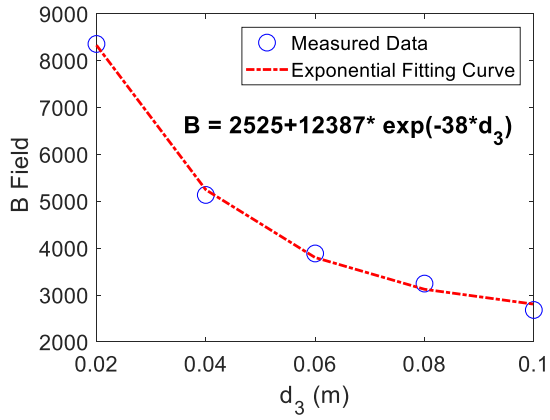

Fig. 14. Coupled magnetic field attenuates with distance between the MWC and the cable.

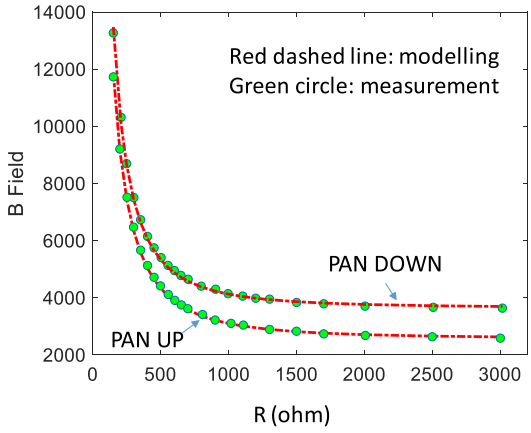

Fig. 15. Coupled magnetic field varies with the impedance between the CMM and the ground.

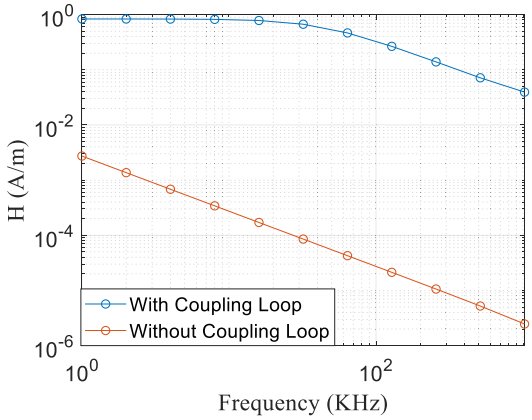

Fig. 16. Simulated magnetic fields at the receiver position for different frequencies: with and without the coupling loop.

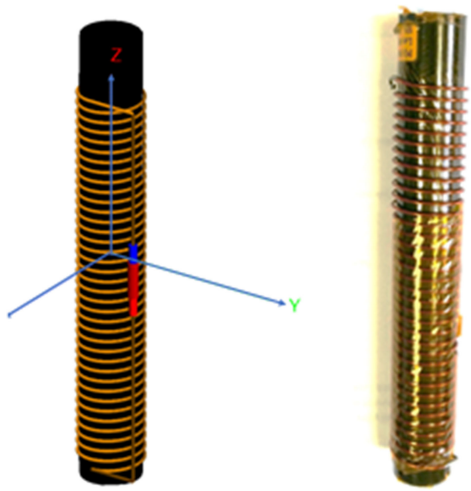

Fig. 17. Simulated ferrite-rod antenna (left) and the actual antenna used in a PDS generator.

Fig. 14 shows how the coupled field varies with the distance between the trailing cable and the MWC, based on the experimental setup given in Fig. 8. Similar to Fig. 11, Fig. 14 shows that the coupled magnetic field decreases exponentially with the distance between the MWC and the trailing cable (i.e., d_3). The result in Fig. 14 suggests that the coupling effect can be dramatically mitigated by keeping the MWC some minimum distance away from the trailing cable.

Fig. 15 shows how the coupled magnetic field varies with the impedance between the CMM and the ground. Based on the experimental setup illustrated in Section IV-E, the resistance of the potentiometer was set to different predetermined values, and the corresponding coupled magnetic field for each resistance value was recorded. This process was repeated for both "PAN DOWN" and "PAN UP" configurations, which varies the impedance between the CMM and the ground by changing the value of X rather than R. The red dashed lines in Fig. 15 are simulated results based on (7) where the two unknown parameters K_0 and X were treated as two fitting parameters to best match the simulated results to the measured results, which are shown as a green circle. It is observed from Fig. 15 that the simulated results agree well with the measured results, indicating that the simplified model presented in (7) is accurate. As expected, the magnetic field coupled from the PDS to the trailing cable quickly decreases with the resistance between the CMM and the ground when the resistance is small (for example, $R < 1000\ \Omega$). For large resistances (1000 Ω or above), however, the coupled field does not vary with the resistance significantly. In addition to resistance, Fig. 15 also shows that the coupled field is influenced by the capacitance between the CMM and the ground. For the same resistance, the "PAN DOWN" configuration produces a stronger coupled field than the "PAN UP" configuration. This can be explained by the fact that raising the pan ("PAN UP") causes the capacitance between the CMM and the ground to decrease, which leads to a decreased coupled field.

B. Simulation Results

Fig. 16 shows a comparison of the simulated magnetic fields (vector sum of the three-axis fields) at the same receiver position for with and without the large coupling loop. It is apparent that the received field with the coupling loop is much stronger than the field at the same location but without the coupling loop. Since the receiver position is located far from

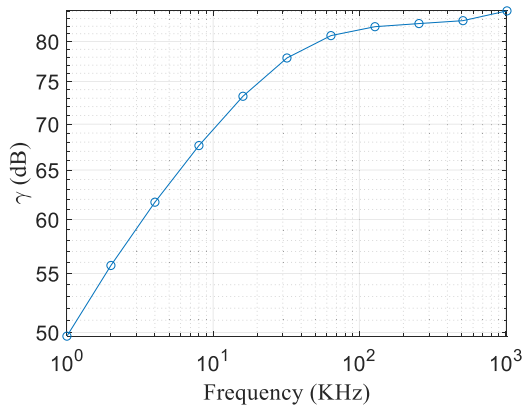

Fig. 18. Coupled to direct signal ratio varies with frequency.

the transmitting antenna, with the presence of the large coupling loop, the magnetic field received by an MWC can be approximately viewed as the coupled field only (i.e., $r_{\rm cp}(t)$). Accordingly, without the presence of the coupling loop, the received signal would be the direct signal $r_{\rm dr}(t)$. As a result, the result in Fig. 16 can be viewed as a comparison between the coupled field and the direct field for different system frequencies.

It should be noted that the source driving the ferrite-rod antenna in the simulation is a voltage source. In other words, the source currents (I_s) for different frequencies are different, given a fixed excitation voltage. To further characterize the influence of frequency on the parasitic coupling, we introduce a new metric: coupled to direct signal ratio, which is defined by: $\boldsymbol{\gamma} = 20 * \mathbf{log}(r_{\rm cp}(t)/r_{\rm dr}(t))$. Lower values $\boldsymbol{\gamma}$ correspond to weaker parasitic coupling and, thus, are more desirable for a PDS. Fig. 18 shows the simulated $\boldsymbol{\gamma}$ for different system frequencies. It is found that $\boldsymbol{\gamma}$ increases with frequencies and then saturates around $f = 100$ KHz. The frequency point where $\boldsymbol{\gamma}$ becomes saturated seems to be closely related to the value of *R* and *C* in (7) and, thus, is strongly dependent on the actual environmental factors where the machine and the PDS is located.

The result in Fig. 18 suggests that lower frequencies would be preferred for a reduced coupling influence. It should be noted that in practice mitigating the parasitic coupling is often not the only consideration when selecting the system frequency for a PDS. There are some other important factors (e.g., the coverage of the direct signal $r_{\rm dr}(t)$ and the electrical noise generated by large machinery in the underground [27]) that must be taken into consideration when designing a PDS.

VII. Conclusion

This article investigates the influence of trailing cables on the performance of magnetic-field-based PDSs. A three-phase model was proposed to describe the coupling process from a PDS generator to a trailing cable, propagation along that cable, and coupling from the cable to an MWC. A series of experiments was designed to study the different factors that control the coupling from a PDS generator to a trailing cable for each of the three phases. It is demonstrated that the coupling effect can significantly enhance the magnetic field received by an MWC and, thus, could potentially cause undesired nuisance alarms. The results show that this coupling effect is primarily controlled by two factors: the distance between the PDS components and the cable [including two distances: 1) the distance between the generator and the cable, and 2) the distance between the cable and the MWC], and the impedance between the cable and the ground. This article shows that the coupling effect can be mitigated by either maintaining some separation distance between the PDS components and the cable or increasing the impedance between the cable and the ground. The minimum separation distances depend on multiple factors and could be different for different mines or for different locations within the same mine. Care should be taken during PDS installation, calibration, and commissioning to understand how coupling affects system performance for a particular installation.

The results and findings presented in this article increase the understanding of the coupling mechanism for a magnetic-field-based PDS and can help PDS manufacturers design better products that are more robust in underground mining environments.

Acknowledgment

The authors would like to thank J. Li, N. Damiano, L.T. Swanson, J. Srednicki, J. Yonkey, and T. Lutz for their help and support with the research reported in this article.

Disclaimer: The findings and conclusions in this report are those of the authors and do not necessarily represent the official position of the NIOSH, Centers for Disease Control and Prevention. Mention of any company or product does not constitute endorsement by NIOSH.

References

[1] MSHA, "Proximity detection/collision warning information from technical support. 2019. [Online]. Available: https://www.msha.gov/proximity-detectioncollision-warning-information-technical-support.

[2] Mine Safety and Health Administration, *Proximity Detection Systems for Continuous Mining Machines in Underground Coal Mines*. vol. 80, 2015. [Online]. Available: https://www.federalregister.gov/documents/2015/01/15/2015-00319/proximity-detection-systems-for-continuous-mining-machines-in-underground-coal-mines

[3] J. Noll, C. DeGennaro, J. Carr, J. Ducarme, and G. Homce, "Causal factors and root causes of underground mobile equipment accidents," in *Proc. Int. Mech. Eng. Congr. Expo.*, Tampa, FL, USA, 2017. [Online]. Available: https://asmedigitalcollection.asme.org/IMECE/proceedings-abstract/IMECE2017/58493/V014T14A007/264603

[4] P. Madhavan, D. A. Wiegmann, and F. C. Lacson, "Automation failures on tasks easily performed by operators undermine trust in automated aids," *Human Factors*, vol. 48, no. 2, pp. 241–256, 2006.

[5] C. Zhou, J. Li, N. Damiano, J. DuCarme, and J. Noll, "Influence of trailing cables on magnetic proximity detection systems," *Mining, Metall. Exploration*, vol. 36, pp. 277–284, 2019.

[6] C. Zhou, B. Whisner, and J. Carr, "An experimental study of magnetic field coupling from proximity detection systems to trailing cables," in *Proc. IEEE Ind. Appl. Soc. Annu. Meeting*, Baltimore, MD, USA, 2010, pp. 1–10.

[7] D. Charnock, "Electromagnetic interference coupling between power cables and sensitive circuits," *IEEE Trans. Power Del.*, vol. 20, no. 2, pp. 668–673, Apr. 2005.

[8] G. Diendorfer, "Induced voltage on an overhead line due to nearby lightning," *IEEE Trans. Electromagn. Compat.*, vol. 32, no. 4, pp. 292–299, Nov. 1990.

[9] S. Op't Land, T. Mandic, M. Ramdani, A. Baric, R. Perdriau, and B. Nauwelaers, "Comparison of field-to-line coupling models: Coupled transmission lines model versus single-cell corrected Taylor model," in *Proc. Int. Symp. Electromagn. Compat.*, 2013, pp. 276–281.

[10] D. Poljak and K. El Khamlichi Drissi, "Electromagnetic field coupling to overhead wire configurations: Antenna model versus transmission line approach," *Int. J. Antennas Propag.*, vol. 2012, 2012, Art. no. 730145.
[11] F. Rachidi, "A review of field-to-transmission line coupling models with special emphasis to lightning-induced voltages on overhead lines," *IEEE Trans. Electromagn. Compat.*, vol. 54, no. 4, pp. 898–911, Aug. 2012.
[12] F. Rachidi and S. Tkachenko, *Electromagnetic Field Interaction With Transmission Lines: From Classical Theory to HF Radiation Effects*. Southampton, U.K.: WIT Press, 2008.
[13] A. A. Smith, "The response of a two-wire transmission line excited by the nonuniform electromagnetic fields of a nearby loop," *IEEE Trans. Electromagn. Compat.*, vol. EMC-16, no. 4, pp. 196–200, Nov. 1974.
[14] Y. Qin, D. E. Brocker, P. L. Werner, D. H. Werner, C. Zhou, and J. Waynert, "Efficient modeling of a small circular loop coupling to a single wire above a lossy half-space," in *Proc. Int. Symp. Antennas Propag. USNC/URSI Nat. Radio Sci. Meeting*, 2015, pp. 1080–1081.
[15] NIOSH, "Technology news 546," in *Medium Frequency Mine Emergency Communications*, N. Damiano, Ed. Pittsburgh, PA, USA: Department of Health and Human Services, Public Health Service, Centers for Disease Control and Prevention, National Institute for Occupational Safety and Health, DHHS (NIOSH), 2011. [Online]. Available: https://www.cdc.gov/niosh/mining/works/coversheet906.html
[16] N. W. Damiano *et al.*, "Simulation and measurement of medium-frequency signals coupling from a line to a loop antenna," *IEEE Trans. Ind. Appl.*, vol. 52, no. 4, pp. 3527–3534, Oct. 2016.
[17] J. Li, J. L. Carr, C. Zhou, M. A. Reyes, and J. D. Noll, "A method for estimating the low frequency coupling characteristics of a ferrite-cored rod antenna to a long conductor," *Prog. Electromagn. Res.*, vol. 75, pp. 193–203, 2018.
[18] C. Zhou, B. G. Whisner, J. L. Carr, and J. Srednicki, "Influence of steel mesh on magnetic proximity detection systems: An experimental study," *Progress Electromag. Res. M*, vol. 90, pp. 89–97, 2020.
[19] C. Zhou and J. Carr, "Modeling the influence of steel mesh on magnetic proximity detection systems (PDSs) in underground coal mines," in *Proc. Prog. Electromagn. Res. Symp.*, 2019, pp. 1837–1844.
[20] J. Li, J. Carr, J. Waynert, and P. Kovalchik, "Environmental impact on the magnetic field distribution of a magnetic proximity detection system in an underground coal mine," *J. Electromagn. Waves Appl.*, vol. 27, no. 18, pp. 2416–2429, 2013.
[21] A. F. Molisch, *Wireless Communications*. Hoboken, NJ, USA: Wiley, 2012.
[22] C. Zhou, J. Li, and J. Carr, "Modeling the magnetic field radiated from a ferrite rod antenna for mining proximity detection systems," in *Proc. Prog. Electromagn. Res. Symp.*, 2018, pp. 496–505.
[23] C. Jobes, J. Carr, and J. DuCarme, "Evaluation of an advanced proximity detection system for continuous mining machines," *Int. J. Appl. Eng. Res.*, vol. 7, no. 6, pp. 649–671, 2012.
[24] J. P. DuCarme, J. L. Carr, and C. C. Jobes, "Proximity detection with selective machine shutdown," presented at the 2015 SME Annu. Meeting and Exhibition, Denver, CO, USA, 2015.
[25] C. Jobes, J. L. Carr, G. T. Homce, and A. K. Smith, "Analysis, conversion, and visualization of survey position and magnetic field strength data for a proximity detection system," presented at the SME Annu. Meeting, Phoenix, AZ, USA, Feb. 21–24, 2016.
[26] J. Li, M. A. Reyes, N. W. Damiano, B. G. Whisner, and R. J. Matetic, "Medium frequency signal propagation characteristics of a lifeline as a transmission line in underground coal mines," *IEEE Trans. Ind. Appl.*, vol. 52, no. 3, pp. 2724–2730, May/Jun. 2016.
[27] W. Schiffbauer, "Active proximity warning system for surface and underground mining applications," *J Mining Eng.*, vol. 54, no. 12, pp. 40–48, 2002.

Chenming Zhou received the Ph.D. degree in electrical engineering from Tennessee Technological University, Cookeville, TN, USA, in 2008.

He is a Senior Research Engineer with the National Institute for Occupational Safety and Health (NIOSH), part of the Centers for Disease Control and Prevention (CDC), under the U.S. Department of Health and Human Services. He has served as a Project Leader and Principal Investigator for a few research projects in the areas of wireless communication and tracking, Internet of Things (IoT), and proximity detection. He also serves as a government Contract Officer Representative (COR) for NIOSH Broad Agency Announcement (BAA) contracts. His research interests include the broad fields of communication and tracking, IoT, and automation with applications in smart mining.

Dr. Zhou is currently an Associate Editor for the *IEEE Antennas and Propagation Magazine*.

Bruce Whisner is an Electronics Technician who served six years with the U.S. Navy, Orlando, FL, USA. He received two years of nuclear power training, and for four years, worked on avionics systems. He started working with Siemens/Robicon in 1997, working with large drive applications, printed circuit boards, and computerized numerical control machines for 13 years. He started working with the National Institute for Occupational Safety and Health, Pittsburgh, PA, USA, in 2010. He has worked on projects related to safer battery testing, proximity detection, medium-frequency propagation, and through-the-earth communication. He has automated data collection processes using LabVIEW.

Mr. Whisner received the Centers for Disease Control Employee of the Month Award in April and the Federal Executive Board Gold Award for Best Technician in 2012.

Jacob Carr received the B.S. and M.S. degrees in mining engineering from the University of Nevada, Reno, NV, USA, in 2006 and 2008, respectivey, where he researched the partial automation of mining equipment, and the Ph.D. degree in energy and mineral engineering from Penn State, State College, PA, USA, in 2019 with research on the introduction of new safety and health interventions.

He leads the Machine Safety team within the Pittsburgh Mining Research Division, National Institute for Occupational Safety and Health, Pittsburgh, PA, USA. He has authored more than 30 publications and has been recognized with several prestigious awards. His research focuses on improving the safety of miners working around machinery at mines.